Sensitivity Analysis

Oliwer Sliczniuk[a,*], Pekka Oinas[a]

[a]Aalto University, School of Chemical Engineering, Espoo, 02150, Finland

ARTICLE INFO

Keywords:
Supercritical extraction
Sensitivity analysis
Mathematical modelling

ABSTRACT

This study aimed to investigate the supercritical extraction process of caraway oil from chamomile flowers. The distributed-parameter model describes the fluid-solid extraction process. The concept of quasi-one-dimensional flow is applied to reduce the number of spatial dimensions. The flow is assumed to be uniform across any cross-section, although the area available for the fluid phase can vary along the extractor. The physical properties of the solvent are estimated from the Peng-Robinson equation of state. A set of laboratory experiments was performed under multiple constant operating conditions: $30-40°C$, $100-200$ bar, and $3.33-6.67\times10^{-5}$ kg/s. Sensitivity analyses play a crucial role in assessing the robustness of the findings or conclusions based on mathematical model. The local sensitivity analysis investigates the influence of infinitely small changes in the inlet temperature, pressure, and flow rate on the extraction yield.

1. Introduction

This study investigates the extraction of essential oil from chamomile flowers (Matricaria chamomilla L.) via supercritical fluid extraction techniques and the modelling of this process. Chamomile is a medicinal herb widely cultivated in southern and eastern Europe—such as Germany, Hungary, France, and Russia. It can be found outside of Europe in Brazil as discussed by Singh et al. [1]. This plant is distinguished by its hollow, bright gold cones, housing disc or tubular florets and surrounded by about fifteen white ray or ligulate florets. Chamomile has been used for its medicinal benefits, serving as an anti-inflammatory, antioxidant, mild astringent, and healing remedy. Chamomile's aqueous extract is widely used to calm nerves and mitigate anxiety, hysteria, nightmares, insomnia, and other sleep-related conditions, according to Srivastava [2]. Orav et al. [3] reported that oil yields from dried chamomile samples ranged from 0.7 to 6.7 mL/kg. The highest yields of essential oil, between 6.1 and 6.7 mL/kg, were derived from chamomile sourced from Latvia and Ukraine, while chamomile from Armenia exhibited a lower oil content of 0.7 mL/kg.

Evaluating the economic viability of the process is essential when choosing the suitable technology for essential oil extraction. Traditional methods, such as distillation and organic solvent extraction, are commonly employed but come with drawbacks. Distillation, for example, involves high temperatures that can lead to the thermal degradation of heat-sensitive compounds. This limitation has led to the increased popularity of alternative techniques like supercritical fluid extraction. Supercritical carbon dioxide is appealing due to its distinctive properties: it is inflammable, non-toxic, and is non-corrosive. CO_2 is the most used supercritical fluid, sometimes modified by co-solvents such as ethanol. Supercritical fluids are capable of exhibiting both gas- and liquid-like properties, allowing for adjustable dissolving power through changes in operating conditions.

The literature offers various mathematical models to describe the extraction of valuable compounds from a biomass. Selecting a model requires a deep understanding of the physical processes, as each model is built on specific assumptions, mass transfer mechanisms and equilibrium dynamics.

The model proposed by Reverchon et al. [4] is the hot ball model, which is based on an analogy to heat transfer and describes an extraction process from solid particles. The model is based on assumptions that that particles contains low quantities of solute and solubility is not a limiting factor.

The Broken-and-Intact Cell model, proposed by Sovova [5], assumes that external surfaces of particles are mechanically disrupted, allowing the solvent's access to the solute in broken cells, while the solute in intact cells remains less accessible due to higher mass transfer resistance.

Reverchon [6] formulated a fluid-solid extraction model where the solute is treated as a single component, governed by internal mass transfer resistance and omitting the effects of external mass transfer, axial dispersion, and variations in fluid density and flow rate throughout the bed.

This work builds upon the linear kinetic model suggested by Reverchon [6], deriving fundamental governing equations to develop a comprehensive model for the chamomile oil extraction process. This model aims for control-oriented simplicity, assuming a semi-continuous operation within a cylindrical vessel. The process involves supercritical solvent being pumped through a fixed bed of finely chopped biomass to extract the solute, followed by separation of the solvent and solute in a flush drum to collect the extract. Parameters such as the pressure (P), feed flow rate (F_{in}) and inlet temperature (T_{in}) are adjustable and measurable, while the outlet temperature (T_{out}) and the amount of product at the outlet can only be monitored. Figure 1 presents a simplified process flow diagram.

This study focuses on finding a process model for the extraction of natural substances from solid materials using supercritical fluids, with a particular emphasis on supercritical CO_2. The approach involves estimating the

*Corresponding author
oliwer.sliczniuk@aalto.fi (O. Sliczniuk)
ORCID(s): 0000-0003-2593-5956 (O. Sliczniuk); 0000-0002-0183-5558 (P. Oinas)

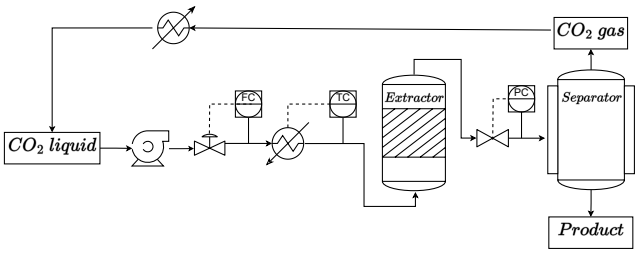

Figure 1: Process flow diagram

solvent properties through thermodynamic relationships and determining the extraction kinetic parameters via a series of experiments conducted under a variety of conditions. The maximum likelihood estimation method is employed solve the parameter estimation problem. Later, the correlations between parameters and operating conditions are found.

This study aims to analyze the influence of changes in operating conditions on the supercritical extraction process described in article 1. The emphasis is put on the effect of the mass flow rate, pressure, and the inlet temperature. The relation between input and output is obtained by applying a sensitivity analysis. Sensitivity analysis examines the impact of varying inputs or model parameters on the system's output. The aim is to understand and to allocate the source of uncertainty in the output to the corresponding inputs or parameters. There are many sensitivity analysis methods, which include but are not limited to those listed below:

- One-at-a-time method
- Derivative-based local methods
- Variance-based methods

Different supercritical extraction models were analyzed using sensitivity analysis. Fiori et al. [7], performed the sensitivity calculations by varying the parameters within their confidence interval and observing how the model results changed. This allows to evaluate the effect of the uncertainties on model predictions. The sensitivity analysis revealed that the particle diameter and the internal mass transfer coefficient are significant for the extraction process. The effect of changing some operative conditions was also investigated, underlining how the solvent flow rate and the seed milling affect the extraction process.

Santos et al. [8], in their work, considered a model of supercritical extraction process for semi-continuous isothermal and isobaric extraction process using carbon dioxide as a solvent. The parametric sensitivity analysis was carried out by applying disturbances of 10% in the values of the normal operation conditions.

Hatami and Ciftci [9] used a one-factor-at-a-time sensitivity analysis to assess the response of NPV concerning variations in both technical and economic variables. Their findings show that the most influential factors on NPV include the price of the extract, the interest rate, the dynamic time of SFE, and the project lifetime.

Poletto and Reverchon [10] provided a general dimensionless model for the supercritical extraction process of vegetable and essential oils and applied a sensitivity analysis. They found that a dimensionless partition coefficient and a dimensionless characteristic time appeared as the most important parameters of the extraction process. The sensitivity calculations were performed by varying the parameters and analyzing the model response.

2. Materials and methods

2.1. Governing equations

Following the work of Anderson [11], the governing equations for quasi-one-dimensional were derived. Quasi-one-dimensional flow refers to a fluid flow scenario assuming that flow properties are uniformly distributed across any given cross-section. This simplification is typically applied in situations where the flow channel's cross-sectional area changes, such as through irregular shapes or partial fillings of an extractor. According to this assumption, velocity and other flow properties change solely in the flow direction.

As discussed by Anderson [12], all flows are compressible but some of them can be treated as incompressible when the Mach number is smaller than 0.3. This assumption leads to the incompressible condition: $\nabla \cdot u = 0$, which is valid for constant density (strict incompressible) or varying density flow. The restraint allows for the removal of acoustic waves, and allows for large perturbations in density and/or temperature. In the 1-D case, the incompressibility condition becomes $\frac{du}{dz} = 0$, so the fluid velocity is constant.

The set of quasi-one-dimensional governing equations in Cartesian coordinates is described by Equations 1 - 3.

$$\frac{\partial\left(\rho_f A_f\right)}{\partial t} + \frac{\partial\left(\rho_f A_f v\right)}{\partial z} = 0 \tag{1}$$

$$\frac{\partial\left(\rho_f v A_f\right)}{\partial t} + \frac{\partial\left(\rho_f A_f v^2\right)}{\partial z} = -A_f \frac{\partial P}{\partial z} \tag{2}$$

$$\frac{\partial\left(\rho_f e A_f\right)}{\partial t} + \frac{\partial\left(\rho_f A_f v e\right)}{\partial z} = -P\frac{\left(A_f v\right)}{\partial z} + \frac{\partial}{\partial z}\left(k\frac{\partial T}{\partial z}\right) \tag{3}$$

where ρ_f is the density of the fluid, A_f is the function which describe change of the cross-section, v is the velocity, P is the total pressure, e is the internal energy of the fluid, t is time and z is the spacial direction.

2.2. Extraction model

2.2.1. Continuity equation

The previously derived quasi-one-dimensional continuity equation (Equation 1) is refined by incorporating a function $A_f = A\phi$. This modification accounts for the variability in the cross-sectional area available for fluid flow. Equation 4 presents this adaptation in the differential form of the continuity equation, capturing the dynamics of the flow as it responds to changes in the cross-section.

$$\frac{\partial(\rho_f \phi)}{\partial t} + \frac{\partial(\rho_f v A\phi)}{\partial z} = 0 \tag{4}$$

where A is the total cross-section of the extractor and ϕ describe porosity along the extractor.

Assuming that the mass flow rate is constant in time, the temporal derivative becomes the mass flux F, and the spatial derivative can be integrated along z as

$$\int \frac{\partial(\rho_f v A\phi)}{\partial z} dz = F \rightarrow F = \rho_f v A\phi \tag{5}$$

To simplify the system's dynamics, it is assumed that F is a control variable and affects the whole system instantaneously (due to $\nabla \cdot u = 0$), which allows finding the velocity profile that satisfies mass continuity based on F, ϕ, and ρ_f.

$$v = \frac{F}{\rho_f A\phi} \tag{6}$$

Similarly, the superficial velocity might be introduced.

$$u = v\phi = \frac{F}{\rho_f A} \tag{7}$$

The fluid density ρ_f can be obtained from an equation of state (Appendix A.1) if temperature and thermodynamic pressure are known along z. The variation in fluid density may occurs due to pressure or a inlet temperature changes.

2.2.2. *Mass balance for the fluid phase*

This equation accounts for the movement of the pseudo-homogeneous fluid phase (Equation 8), which is constrained to the axial direction due to the quasi-one-dimensional approach that considers changes in the void fraction. It is also assumed that the thermodynamic pressure remains constant throughout the device. The analysis further simplifies the flow dynamics by disregarding the boundary layer near the extractor's inner wall, leading to a uniform velocity profile across any cross-section perpendicular to the axial direction. Given that the solute concentration in the solvent is negligible, the fluid phase is described as pseudo-homogeneous, with properties identical to the solvent itself. Thus, the mass balance equation include convection, diffusion, and kinetic terms to represent the fluid phase behaviour.

$$\frac{\partial c_f}{\partial t} + \frac{1}{\phi}\frac{\partial\left(c_f u\right)}{\partial z} = \frac{1-\phi}{\phi} r_e + \frac{1}{\phi}\frac{\partial}{\partial z}\left(D_e^M \frac{\partial c_f}{\partial z}\right) \tag{8}$$

c_f represents the solute's concentration in the fluid phase, r_e is a mass transfer kinetic term, and D_e^M is the axial diffusion coefficient.

2.2.3. *Mass balance for the solid phase*

The solid phase is considered to be stationary, without convection and diffusion terms in the mass balance equation (Equation 9). Therefore, the only significant term in this equation is the kinetic term (as defined in Equation 10), which connects the solid and fluid phases. The extract is represented by a single pseudo-component for simplicity.

$$\frac{\partial c_s}{\partial t} = \underbrace{r_e}_{\text{Kinetics}} \tag{9}$$

2.2.4. *Kinetic term*

As the solvent flows through the bed, CO_2 molecules diffuse into the pores and adsorb on the particle surface to form an external fluid film around the solid particles due to the solvent-solid matrix interactions. The dissolved solute diffuses from the particle's core through the solid-fluid interface, the pore, and the film into the bulk. Figure 2 shows the mass transfer mechanism, where the mean solute concentration in the solid phase is denoted as c_s and the equilibrium concentrations at the solid-fluid interface are denoted as c_s^* and c_p^*, respectively, for solid and fluid phases. The concentration of the solutes in the fluid phase in the center of the pore is denoted as c_p. As the solute diffuses through the pore, its concentration changes and reaches c_{pf} at the opening of the pore. Then the solute diffuses through the film around the particle and reaches bulk concentration c_f. The two-film theory describes the solid-fluid interface inside the pore. The overall mass transfer coefficient can be determined from the relationship between the solute concentration in one phase and its equilibrium concentration.

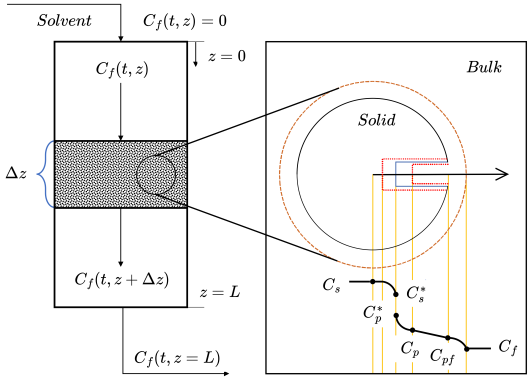

Figure 2: The mass transfer mechanism

Bulley et al. [13] suggests a process where the driving force for extraction is given by the difference between the concentration of the solute in bulk, c_f, and in the center of the pore, c_p^*. The concentration c_p^* is in equilibrium with c_s according to an equilibrium relationship. The rate of extraction is thus $r_e\left(c_f - c_p^*(c_s)\right)$.

On the other hand, Reverchon [6] proposes a driving force given by the difference between c_s and c_p^*.Concentration c_p^* is determined by an equilibrium relationship with c_f and the extraction rate given by Equation 10

$$r_e = \frac{D_i}{\mu l^2}\left(c_s - c_p^*\right) \tag{10}$$

where μ is sphericity, l a characteristic dimension of particles and can be defined as $l = r/3$, r is the mean particle radius, ρ_s is the solid density, D_i corresponds to the overall diffusion coefficient and c_P^* is a concentration at the solid-fluid interface (which according to the internal resistance model is supposed to be at equilibrium with the fluid phase).

According to Bulley et al. [13], a linear equilibrium relationship (Equation 11) can be used to find an equilibrium concentration of the solute in the fluid phase c_f^* is based on the concentration of the solute in the solid phase c_s.

$$c_f^* = k_p c_s \tag{11}$$

The volumetric partition coefficient k_p acts as an equilibrium constant between the solute concentration in one phase and the corresponding equilibrium concentration at the solid-fluid interphase. According to Spiro and Kandiah [14], k_p can be expressed through the mass partition coefficient k_m.

$$k_m = \frac{k_p \rho_s}{\rho_f} \tag{12}$$

According to Reverchon [6], the kinetic term becomes

$$r_e = -\frac{D_i}{\mu l^2}\left(c_s - \frac{\rho_s c_f}{k_m \rho_f}\right) \tag{13}$$

2.2.5. Uneven solute's distribution in the solid phase

Following the idea of the Broken-and-Intact Cell (BIC) model (Sovova [15]), the internal diffusion coefficient D_i is consider to be a product of the reference value of D_i^R and the exponential decay function γ, as given by Equation 14.

$$D_i = D_i^R \gamma(c_s) = D_i^R \exp\left(\Upsilon\left(1 - \frac{c_s}{c_{s0}}\right)\right) \tag{14}$$

where the Υ describe the curvature of the decay function. Equation 15 describes the final form of the kinetic term

$$r_e = -\frac{D_i^R \gamma}{\mu l^2}\left(c_s - \frac{\rho_s c_f}{k_m \rho_f}\right) \tag{15}$$

Such a formulation limits the availability of the solute in the solid phase. Similarly to the BIC model, if solute is assumed to be contained in the cells, a part of which is open because the cell walls were broken by grinding, and the rest remains intact. The diffusion of the solute from a particle's core takes more time compared to the diffusion of the solute located close to the outer surface. Considering that the internal diffusion coefficient decay as the concentration of the solute in the solid decrease. As the value of the c_s decrease over time, the exponential term approach unity and $\lim_{c_s \to 0} D_i = D_i^R$. Coefficient D_i^R can be interpreted as the internal diffusion coefficient at vanishing gradient.

Alternatively, the decay function γ can be consider with respect to the Shrinking Core model presented by Goto et al. [16], where the particle radius change as the amount of solute in the solid phase decrease. As the particle size decrease due to dissolution, the diffusion path increase which makes the diffusion slower and reduce the value of a diffusion coefficient. The same analogy can be apply to the Equation 14 to explain the change of the diffusion coefficient.

2.2.6. Heat balance

The heat balance equation describe the evolution of the internal energy in the system and it is given by Equation 16

$$\frac{\partial\left(\rho_f h A_f\right)}{\partial t} = -\frac{\partial\left(\rho_f h A_f v\right)}{\partial z} + \frac{\partial\left(P A_f\right)}{\partial t} + \frac{\partial}{\partial z}\left(k\frac{\partial T}{\partial z}\right) \tag{16}$$

The main advantage of this formulation is the presence of term $\partial P/\partial t$, which directly affects the system through the change of thermodynamic pressure (which is a control variable).

If the value of enthalpy h is known from the time evolution of the energy equation, and pressure P is known from measurement, then the temperature T can be reconstructed based on the departure function. The departure function is a mathematical function that characterizes the deviation of a thermodynamic property (enthalpy, entropy, and internal energy) of a real substance from that of an ideal gas at the same temperature and pressure. The departure function is defined as the difference between the value of a thermodynamic property for a real fluid and the corresponding value for an ideal gas at the same temperature and pressure. They are computed by integrating a function that depends on the equation of state and its derivatives. As presented by Gmehling et al. [19], for the Peng-Robinson equation of state, the enthalpy can be defined by Equation 17.

$$h - h^{id} = RT\left[T_r(Z-1) - 2.078(1+\kappa)\sqrt{\alpha(T)}\ln\left(\frac{Z + \left(1+\sqrt{2}\right)B}{Z + \left(1-\sqrt{2}\right)B}\right)\right] \tag{17}$$

Equation 17 requires an reference sate, which is assumed to be $T_{ref} = 298.15$[K] and $P_{ref} = 1.01325$[bar].

A root-finder can be used to find a value of temperature, which minimizes the difference between the value of enthalpy coming from the heat balance and the departure functions. The root fining procedure to repeated at every time step to find a local temperature along spatial direction z.

$$\underbrace{h(t,x)}_{\text{Heat balance}} = \underbrace{h\left(T, P, \rho_f(T,P)\right)}_{\text{Departure function}} \tag{18}$$

2.2.7. Pressure term

The pressure term in the energy equation, given by Equation 16, describes the change of the thermodynamic pressure with respect to time. As discussed above, the thermodynamic pressure is nearly constant in space due to the small pressure wave propagation that occurs at the speed of sound. Under such conditions, the term $\partial P/\partial t$ can be approximated by an ordinary differential equation, which describes the instantaneous change of pressure in the system. The pressure (P) in the system is considered a state variable, while the pressure in the new time-step (P_{in}) is considered a control variable.

$$\frac{\partial P}{\partial t} \approx \frac{P - P_{in}}{\Delta t} \tag{19}$$

Such a simplified equation takes into account the pressure change in the energy balance, but the dynamics are simplified and do not consider the effects of pressure losses. In a real system, the dynamics of pressure change would depend on a pump used in an extraction system, as well as a back-pressure regulator used to control an outlet valve.

2.2.8. Extraction yield

The process yield is calculated according to Equation 20 as presented by Sovova et al. [20]. The measurement equation evaluates the solute's mass at the extraction unit's outlet and sums it up. The integral form of the measurement

(Equation 20) can be transformed into the differential form (Equation 21) and augmented with the process model.

$$y = \int_{t_0}^{t_f} \frac{F}{\rho_f} c_f \Big|_{z=L} dt \tag{20}$$

$$\frac{dy}{dt} = \frac{F}{\rho_f} c_f \Big|_{z=L} \tag{21}$$

2.2.9. Initial and boundary conditions

It is assumed that the solvent is free of solute at the entrance of the extractor and that all the solid particles have the same initial solute content c_{s0}. As the residence time is much shorter than the sampling time, the initial state estimate for the concentration of the solute in the fluid phase would be not reliable. Considering that it is assumed that the $c_{f0} = 0$ and that the system is isothermal (described by h_0). The initial and boundary conditions are define as follow:

$$\begin{array}{lll} c_f(t=0,z) = 0 & c_s(t=0,z) = c_{s0} & h(t=0,z) = h_0 \\ \dfrac{\partial c_f(t,z=L)}{\partial x} = 0 & c_f(t,z=0) = 0 & c_s(t,z=\{0,L\}) = 0 \\ \dfrac{\partial h(t,z=L)}{\partial x} = 0 & P(t,z=0) = 0 & y(0) = 0 \end{array}$$

2.2.10. Discretization methods

The method of lines is used to transform the process model equations into a set of ODEs denoted as $G(x;\Theta)$. The backward finite difference is used to approximate the first-order derivative, while the central difference scheme is used to approximate the second-order derivative z-direction. The length of the fixed bed is divided into N_z equally distributed points in z-direction. The state-space model after the discretization is denoted as x and defines as follow:

$$\dot{x} = \frac{dx}{dt} = \begin{bmatrix} \frac{dc_{f,1}}{dt} \\ \vdots \\ \frac{dc_{f,N_z}}{dt} \\ \hline \frac{dc_{s,1}}{dt} \\ \vdots \\ \frac{dc_{s,N_z}}{dt} \\ \hline \frac{dh_1}{dt} \\ \vdots \\ \frac{dh_{N_z}}{dt} \\ \hline \frac{dP}{dt} \\ \hline \frac{dy}{dt} \end{bmatrix} = \underbrace{\begin{bmatrix} G_1\left(c_f, c_s, h; \Theta\right) \\ \vdots \\ G_{N_z}\left(c_f, c_s, h; \Theta\right) \\ \hline G_{N_z+1}\left(c_f, c_s, h; \Theta\right) \\ \vdots \\ G_{2N_z}\left(c, c_s, h; \Theta\right) \\ \hline G_{2N_z+1}\left(c_f, c_s, h; \Theta\right) \\ \vdots \\ G_{3N_z}\left(c_f, c_s, h; \Theta\right) \\ \hline G_{3N_z+1}\left(c_f, c_s, h; \Theta\right) \\ \hline G_{3N_z+2}\left(c_f, c_s, h; \Theta\right) \end{bmatrix}}_{G(x;\Theta)}$$

where $x \in \mathbb{R}^{N_x=3N_z+2}$ and $\Theta \in \mathbb{R}^{N_\Theta=N_\theta+N_u}$, N_θ is the number of parameters, N_u is the number of control variables.

For a derivative to be conservative, it must form a telescoping series. In other words, after the addition of all terms coming from the discretization over a grid, only the boundary terms should remain, and the artificial interior points should cancel out. The discretization is applied to the conservative form of the model to ensure mass conservation.

2.3. Sensitivity Analysis

Local derivative-based methods involve taking the partial derivative of the output with respect to an input parameter. This set of derivatives, known as sensitivity equations, is solved simultaneously with the process model. The sensitivity analysis aims to investigate how responsive the solution is for the perturbation of the parameter p. As discussed by Dickinson and Gelinas [21], the sensitivity analysis can be used to determine the influence of the uncertainty on the solution of the original system. A sensitivity analysis can be used to distinguish sensitive parameters from insensitive ones, which might be helpful for model reduction. Finally, from a control engineering point of view, the sensitivity analysis allows sorting the control variables with respect to the level of effort required to change the model's output.

As presented in the work of Maly and Petzold [22], the sensitivity analysis equations($\dot{Z}$) are developed by taking the total derivative of the state vector x with respect to parameters p, where p is a subset of the parameter space θ.

$$Z(x(t);p) = \frac{dx(t)}{dp} \tag{22}$$

The new system of equations can be obtained by taking derivatives of Z with respect to time t and applying the chain rule.

$$\dot{Z}(x(t);p) = \frac{dZ(x(t);p)}{dt} = \frac{d}{dt}\left(\frac{dx(t)}{dp}\right) = \frac{d}{dp}\left(\frac{dx(t)}{dt}\right) = \frac{dG(x(t);p)}{dp} \tag{23}$$

The sensitivity equation can be obtained by applying the definition of the total derivative to the Equation 23.

$$\frac{dG(x(t);p)}{dp} = \underbrace{\frac{\partial G(x(t);p)}{\partial x(t)}}_{J_x(x(t);p)} \underbrace{\frac{\partial x(t)}{\partial p}}_{S(x(t);p)} + \underbrace{\frac{\partial G(x(t);p)}{\partial p}}_{J_p(x(t);p)} \tag{24}$$

The sensitivity Equation 24 is solved simultaneously with the original system and is made of three terms: jacobian $J_x(x(t);p)$, sensitivity matrix $S(x(t);p)$ and jacobian $J_p(x(t);p)$. The jacobian $J_x(x(t);p)$ represents the matrix of equations of size $N_x \times N_x$, where each equation $J_x(n_x, n_x)$ is the derivative of process model equations $G_{n_x}(x(t);p)$ with respect to the state variable x_{n_p}.

$$J_x(x(t);p) = \begin{pmatrix} \frac{\partial G_1(x(t);p)}{\partial x_1(t)} & \frac{\partial G_1(x(t);p)}{\partial x_2(t)} & \cdots & \frac{\partial G_1(x(t);p)}{\partial x_{N_x}(t)} \\ \frac{\partial G_2(x(t);p)}{\partial x_1(t)} & \frac{\partial G_2(x(t);p)}{\partial x_2(t)} & \cdots & \frac{\partial G_2(x(t);p)}{\partial x_{N_x}(t)} \\ \vdots & \vdots & \ddots & \vdots \\ \frac{\partial G_{N_x}(x(t);p)}{\partial x_1(t)} & \frac{\partial G_{N_x}(x(t);p)}{\partial x_2(t)} & \cdots & \frac{\partial G_{N_x}(x(t);p)}{\partial x_{N_x}(t)} \end{pmatrix} \tag{25}$$

The sensitivity matrix $S(x(t);p)$ represents the matrix of equations of size $N_x \times N_p$, where each subequation $S(n_x, n_p)$ is the derivative of the state variable x_{n_x} with respect to the parameter p_{n_p}.

$$S(x(t);p) = \begin{pmatrix} \frac{\partial x_1(t)}{\partial p_1} & \frac{\partial x_1(t)}{dp_2} & \cdots & \frac{dx_1(t)}{\partial p_{N_p}} \\ \frac{\partial x_2(t)}{\partial p_1} & \frac{\partial x_2(t)}{dp_2} & \cdots & \frac{dx_2(t)}{\partial p_{N_p}} \\ \vdots & \vdots & \ddots & \vdots \\ \frac{\partial x_{N_x}(t)}{\partial p_1} & \frac{\partial x_{N_x}(t)}{dp_2} & \cdots & \frac{\partial x_{N_x}(t)}{dp_{N_p}} \end{pmatrix} \tag{26}$$

The jacobian $J_p(x(t);p)$ represents the matrix of equations of size $N_x \times N_p$, where each subequation $J_p(n_x, n_p)$ is the partial derivative of the process model equation F_{n_x} with respect to the parameter p_{n_p}.

$$J_p(x(t);p) = \begin{pmatrix} \frac{\partial G_1(x(t);p)}{\partial p_1} & \frac{\partial G_1(x(t);p)}{\partial p_2} & \cdots & \frac{\partial G_1(x(t);p)}{\partial p_{N_p}} \\ \frac{\partial G_2(x(t);p)}{\partial p_1} & \frac{\partial G_2(x(t);p)}{\partial p_2} & \cdots & \frac{\partial G_2(x(t);p)}{\partial p_{N_p}} \\ \vdots & \vdots & \ddots & \vdots \\ \frac{\partial G_{N_x}(x(t);p)}{\partial p_1} & \frac{\partial G_{N_x}(x(t);p)}{\partial p_2} & \cdots & \frac{\partial G_{N_x}(x(t);p)}{\partial p_{N_p}} \end{pmatrix} \tag{27}$$

The combined system containing the original set of equations $G(x(t);p)$ and sensitivity equations can be formulated as $\mathbf{G}(x(t);p)$. The size of $\mathbf{G}(x(t);p)$ is equal to $N_s = N_x(N_p + 1)$.

$$\mathbf{G}(x(t);p) = \begin{bmatrix} G(x(t);p) \\ J_x(x(t);p)S(x(t);p) + J_p(x(t);p) \end{bmatrix} \tag{28}$$

The initial conditions are described as

$$\mathbf{G}\left(x(t_0);p\right) = \left[x(t_0), \quad \frac{\mathrm{d}x(t_0)}{dp_1}, \quad \cdots, \quad \frac{dx(t_0)}{dp_{N_p}}\right]^T \tag{29}$$

The sensitivity analysis of the output function can be performed with respect to parameters p. The output function $g(x(t))$ returns $y(t)$. By taking a total derivative of $y(t)$ with respect to p, the new sensitivity equation can be found.

$$\frac{dy(t)}{dp} = \frac{dg(x(t))}{dp} = \frac{\partial g(x(t))}{\partial x(t)}\frac{\partial x(t)}{\partial p} + \frac{\partial g(x(t))}{\partial p} \tag{30}$$

3. Results

This work investigates the influence of inlet temperature, pressure, and mass flow rate on the state space and the extraction yield. The process model and parameters have been discussed in article 1. The process model was calibrated on the set of experiments obtained at different operating conditions, $30-40°C$, 100 – 200 bar, and $3.33-6.67\times10^{-5}$ kg/s. The sensitivity analysis has been performed assuming that the system operates at $35°C$, 150 bar and 5 $\times10^{-5}$ kg/s.

3.1. Flow rate

The increase in the mass-flow rate affects the system simultaneously along the spatial direction by increasing the velocity but without affecting the thermodynamic state of the fluid. As a result, Figure 3 indicates that the system's pressure remains unaffected by changes in the flow rate.

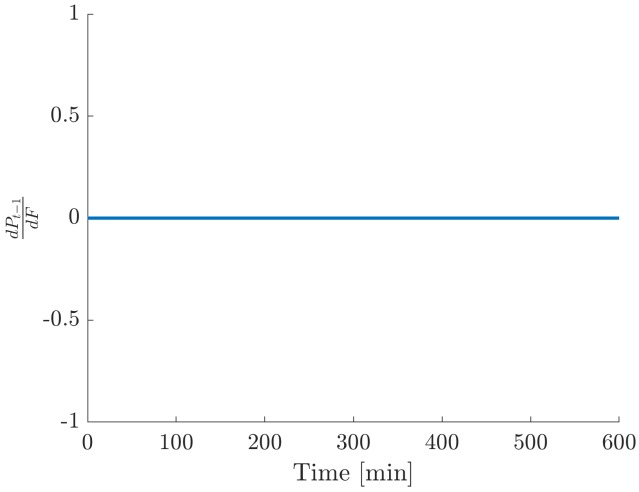

Figure 3: The effect of F change on P

It is important to note that h represents enthalpy but not total enthalpy, thus excluding kinetic energy. As a consequence of the modelling assumptions, changes in h and ρ occur in response to changes in pressure or temperature, which explains no deviation of $h \times \rho$ in Figure 4.

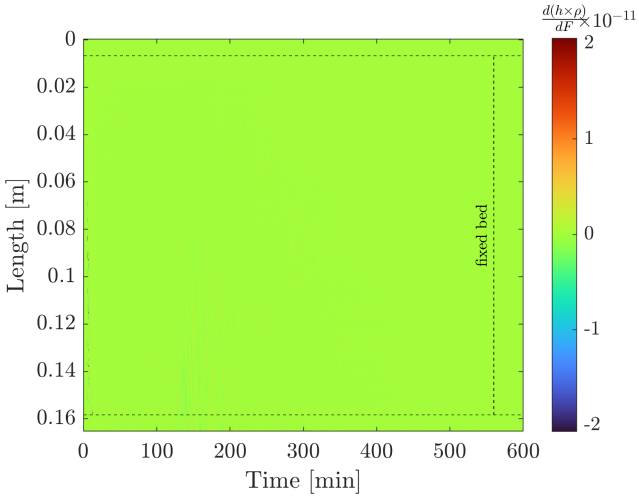

Figure 4: The effect of F change on $h \times \rho$

Figure 5 visualizes how the solute concentration in the solid phase is affected by the mass flow change. It is postulated that with an increase in the mass flow rate, the concentration gradient becomes larger leading to an accelerated decrease of the solute from solid particles and it is characterized by negative sensitivity values. Gradually, the sensitivities decrease until they reach minimum values and the effect of mass flow rate on extraction is most significant.

As the extraction progresses, the sensitivity values become less negative, moving towards zero. This gradual change corresponds to the decreasing concentration of the

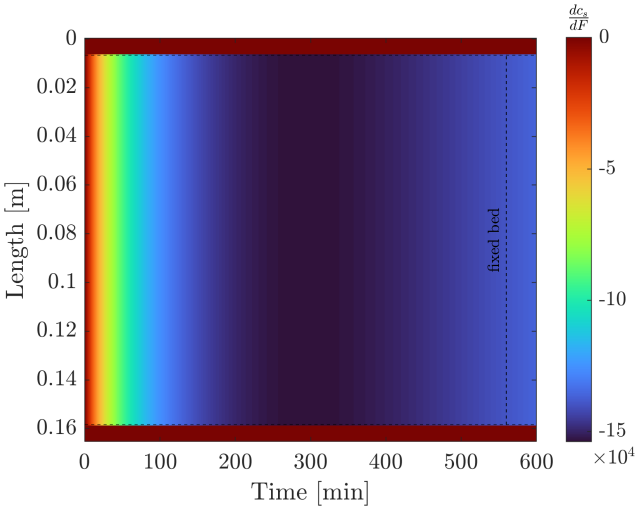

Figure 5: The effect of F change on C_s

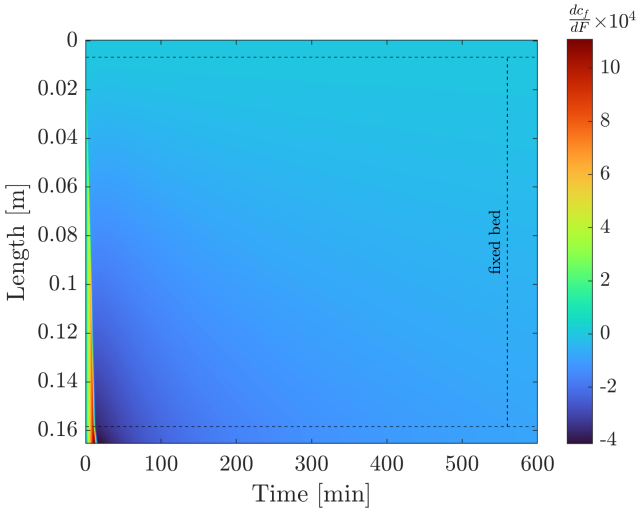

Figure 6: The effect of F change on C_f

solute in the solid phase, which results in a diminishing concentration gradient and, consequently, a reduction in the rate of extraction. The sensitivity approaching zero suggests that the driving force for mass transfer is decreasing as the solute is being depleted. The asymptotic behaviour can be interpreted as a point where the remaining solute concentration in the solid phase is minimal and becomes less dependent on the mass flow rate. At this stage, other factors, such as internal diffusion within the solid matrix or equilibrium limitations, may limit the extraction rate.

The Figure 6 depicts the sensitivity of the solute concentration in the fluid phase to the flow rate within a supercritical fluid extraction system. In the initial phase of the extraction, the sensitivities near the inlet are negligible, as characterized by values close to zero. This indicates a minimal initial response to changes in the flow rate, which could be due to the presence of an high concentration gradient, allowing the fluid phase to rapidly reach solute regardless of the flow rate.

As the extraction progresses, positive sensitivities emerge along the length of the extractor and form the concentration front that moves in the flow direction. This front represents the increased movement of the solute with the fluid phase as the flow rate increases, suggesting an enhanced mass transfer due to the elevated velocity of the supercritical fluid. Following the positive front, there is an emergence of a front characterized by negative sensitivities. This trend illustrates a diminishing solute concentration in the fluid phase, and it reflects a point in the extraction where the solute availability in the solid phase becomes a limiting factor; the depletion of solute reduces the concentration gradient, thereby decelerating the extraction rate.

Toward the end of the extraction process, the sensitivities are shown to increase from their negative values towards zero. This asymptotic approach suggests that the system is reaching a kinetic regime where further increases in the flow rate have a low impact on the solute concentration in the fluid phase. This behavior reflects a physical limit where the remaining solute in the solid phase is insufficient to sustain a high concentration in the fluid phase, regardless of the flow rate. It indicates a terminal phase of the extraction process where the available solute has been largely exhausted, and the system response to changes in flow rate is inherently constrained by the depletion of extractable material.

The Figure 7 depicts the sensitivity of the extraction yield to variations in mass flow rate as a function of time. The curve's initial rise to a peak followed by a decline conveys the dynamic relationship between the mass flow rate and the extraction yield within the supercritical extraction process.

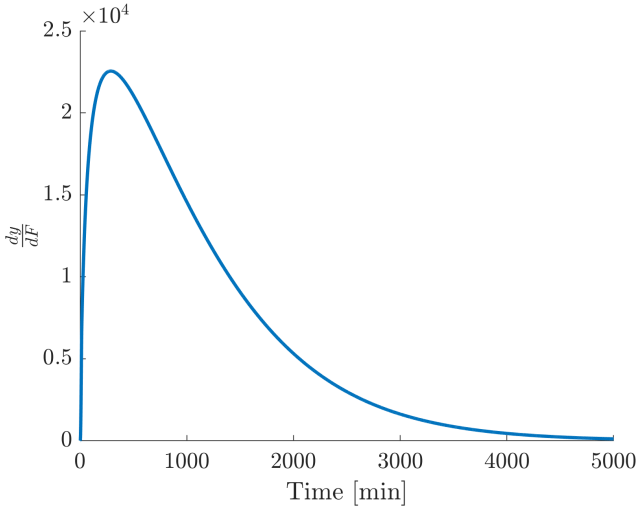

Figure 7: The effect of F change on $y(t)$

In the early phase, the sensitivity is minimal, denoting that adjustments to the mass flow rate have a negligible influence on the yield. This can be attributed to the initial phase of the extraction, where the mass transport mechanisms are mainly controlled by a high concentration gradient.

As the process evolves, the curve's ascent to its apex signifies a period during which the extraction yield becomes increasingly sensitive to the mass flow rate. This is likely due to the mass flow rate enhancing the convective transport of solute, maximizing the extraction efficiency. At this stage, the solute transfer from the solid to the fluid phase is most responsive to changes in flow rate.

However, the curve's descent past the peak suggests a diminishing return on sensitivity with further increases in mass flow rate. The decrease indicates a transitional phase where the extraction process likely encounters diffusion limitations or a depletion of readily extractable solute. The concentration gradient, which drives the mass transfer, may be reduced due to the depletion of solute in the solid phase, or the system may be experiencing diffusive resistances that limit the rate at which solute can be delivered to the fluid phase.

The asymptotic approach to zero sensitivity towards the end of the curve reflects a regime where the yield is no longer significantly influenced by the mass flow rate. At this juncture, the extraction process has likely exhausted the available solute, and any further increase in mass flow rate does not result in a proportional increase in yield. The extraction system has reached a point of saturation or equilibrium where the mass transfer is limited by factors other than flow rate, such as the intrinsic properties of the solute or the matrix, indicating that the system has achieved as much extraction as is practically feasible under the given conditions.

The curve captures the non-linear and transient nature of the extraction yield's response to the mass flow rate, underscoring the importance of optimizing flow rates over the duration of the extraction to maximize yield. It also highlights the multifaceted dependencies and constraints inherent in supercritical fluid extraction processes, such as mass transfer rates, solute availability, and diffusion limitations.

3.2. Pressure

As discussed in Chapter 2.1, a small pressure wave propagates at the speed of sound relative to the flow. If the flow velocity is relatively low, all pressure changes are hydrodynamic (resulting from velocity motion) rather than thermodynamic. The Low Mach-number assumption leads to instant propagation of the thermodynamic pressure throughout the system. This assumption allows considering a single pressure value for the entire system, as all changes occur simultaneously within the machine. Figure 8 illustrates a step function representing the pressure change.

According to Equation 16, the pressure change directly affects the quantity $h \times \rho$ through $\partial(P(t)A_f)/\partial t$, leading to the step change along the whole system, as presented in Figure 9. The uniform response across the entire extraction column length and time, represented by the homogeneously dark red color, indicates that the entire system experiences an immediate and uniform change in enthalpy density in response to pressure changes. This is consistent with the

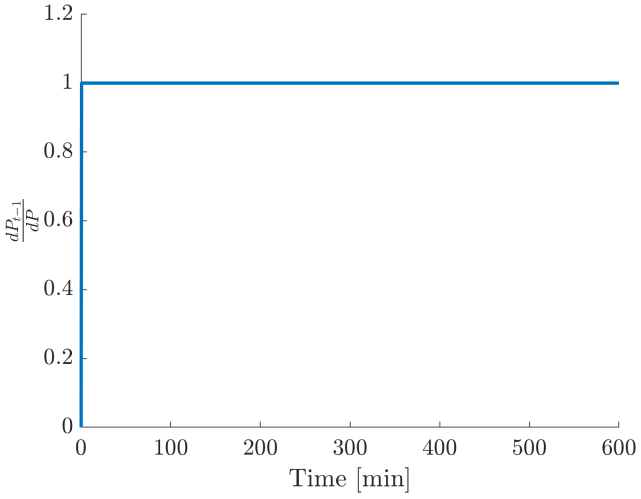

Figure 8: The effect of P change on P in the system

physical expectation that pressure changes should equilibrate rapidly throughout the fluid phase due to the high compressibility of supercritical fluids.

Regarding the boundary conditions, by applying the Dirichlet boundary conditions(mean setting a fixed temperature at the system boundary) can leads to a possible thermal gradient within the system if the initial temperatures differ. In contrast, Neumann boundary conditions would dictate that the heat flux at the boundaries be held constant, ensuring temperature uniformity between the inlet and the rest of the extractor. In case of this work, the Neumann boundary conditions have been applied, as indicated by the uniform response in enthalpy density, implying that there is no temperature gradient caused by a heat front propagating through the system. Instead, the temperature within the extractor is instantaneously and evenly matched to that at the inlet.

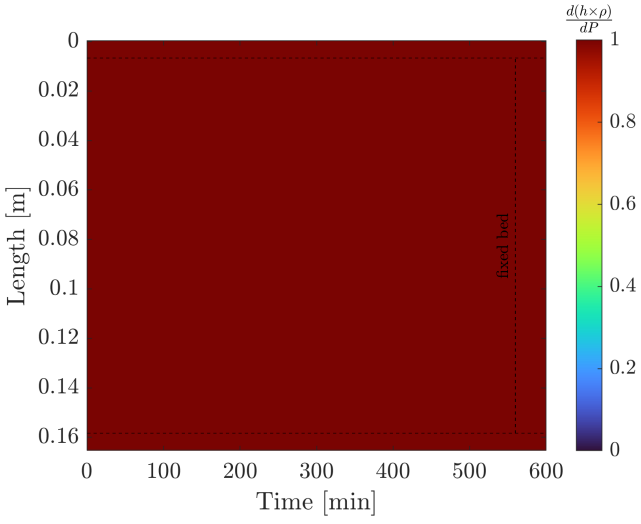

Figure 9: The effect of P change on $(h \times \rho)$ in the system

The provided figure showcases the sensitivity of the solute concentration in the solid phase with respect to changes

in pressure throughout a fixed bed in a supercritical fluid extraction process.

As discussed in Chapter 2.2.1, the velocity of a fluid is inversely related to its density, which suggests that with higher fluid density—often associated with increased pressure—the velocity decreases. This leads to an extended residence time of the fluid within the system. The lower velocity afforded by increased pressure allows for a longer interaction between the solute and the solvent, potentially a higher concentration of solute in the fluid phase.

Simultaneously, pressure changes alter the fluid's thermodynamic state, affecting the extraction process's kinetics. These changes are characterized by correlations (article 1), such as the increase of the diffusion coefficient D_i^R with fluid density. A higher D_i^R indicates enhanced mass transfer capabilities, contributing to an increased rate of extraction.

Figure 10 captures these dual effects on the solute concentration within the solid matrix. Initially, the system response is low due to a high concentration gradient. When the concentration gradient starts to diminish, high sensitivities reveal that changes in pressure have a more pronounced effect. This is consistent with the fluid's higher density and lower velocity, resulting in more effective mass transfer from the solid to the fluid phase.

Over time, the pressure change has a lower effect and the sensitivities decay. This trend signifies that the impact of pressure on solute concentration is diminishing, likely due to the depletion of the solute in the solid phase over time. The decreasing concentration gradient suggests that the solute availability becomes a limiting factor in the extraction process.

Eventually, sensitivities asymptotically approach zero. The solute concentration in the solid phase has been reduced, and further changes in pressure do not influence the remaining concentration. This behaviour reflects that in the later extraction phase, the kinetics of extraction are dominated by the reduced availability of the solute rather than the conditions of the supercritical fluid.

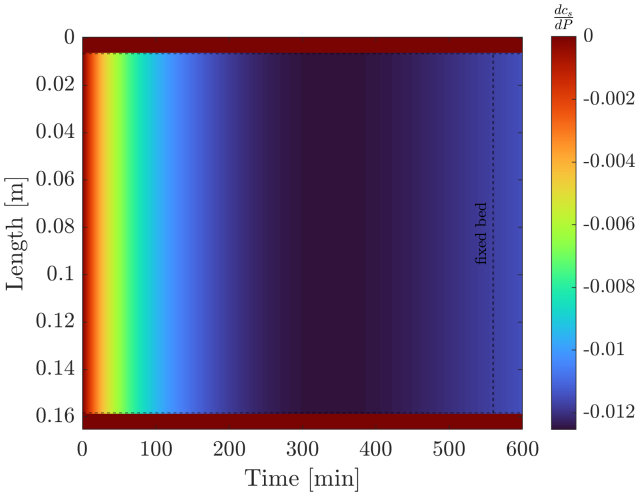

Figure 10: The effect of P change on C_s

Figure 11 shows the sensitivity of the solute concentration in the fluid phase as a function of pressure changes throughout the supercritical extraction column's length and over the extraction process's duration. An increase in pressure typically enhances the solute's solubility, resulting in its heightened presence in the supercritical fluid, which is seen as a leading front moving through the system. Due to the diffusion effect, the gradient becomes more dispersed in regions beyond the fixed bed. Following this, the formation of a trailing front characterized by decreasing sensitivities can be observed. This trailing front can be explained by the decrease in the concentration gradient as the solute is increasingly extracted and the available concentration within the solid phase diminishes. As seen in the figure, sensitivities are declining towards zero. This asymptotic trend suggests the driving force for the mass transfer—the concentration gradient—has been minimized, and changes in pressure no longer significantly impact the solute concentration in the fluid phase.

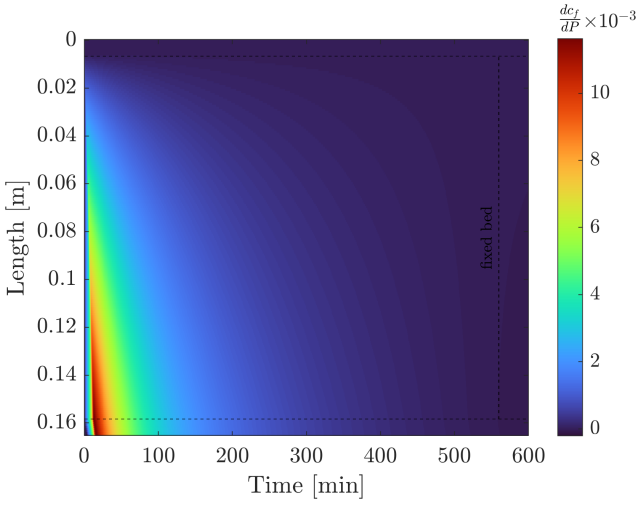

Figure 11: The effect of P change on C_f

Figure 12 illustrates the temporal evolution of the extraction yield's sensitivity to changes in pressure within a supercritical fluid extraction system.

Initially, the curve displays an almost flat profile, suggesting a latency in the system's response to pressure changes. A minor initial decrease in sensitivity, indicated by a slight dip below zero, may arise due to a decrease in the velocity of the fluid phase. For a constant mass flow rate, an increase in fluid density due to heightened pressure results in a lower fluid velocity, potentially leading to this reduced sensitivity.

As the process continues, the curve ascends sharply, indicating a positive yield response to pressure. This increase in sensitivity can be associated with the enhanced solubility and mass transfer capabilities imparted by higher pressures, improving the rate at which solute is extracted into the fluid phase. The peak in dy/dP reflects the most responsive period of the system, where pressure changes are highly effective in improving yield.

Beyond the peak, the sensitivity declines, converging towards zero. This descending curve represents a depletion phase: as the available solute in the solid phase diminishes, the potential for further increasing the yield through pressure alone is reduced. The remaining solute concentration becomes a limiting factor, and the mass transfer driving force, initially augmented by pressure, no longer plays a dominant role.

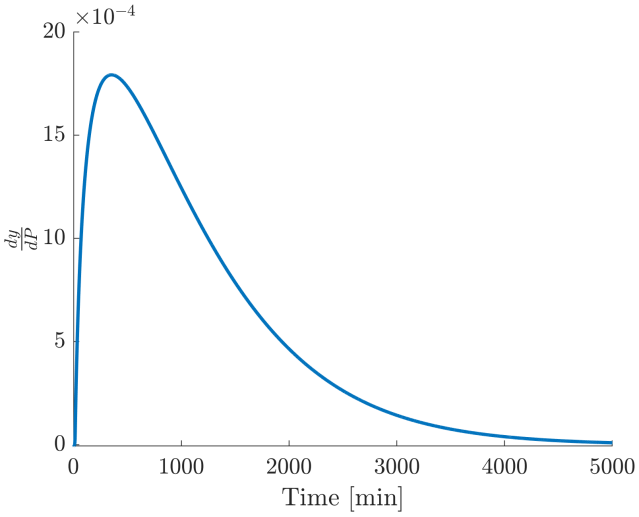

Figure 12: The effect of P change on $y(t)$

3.3. Inlet temperature

The sensitivity analysis of the inlet temperature differs from the two cases presented earlier because the perturbation does not affect the entire system instantaneously; instead, it propagates through it.

Figure 13 presents the sensitivity of the system's pressure response to changes in the inlet temperature over time during a supercritical fluid extraction process. The flat curve, hovering at zero, indicates a system where the pressure does not exhibit any response to changes in the inlet temperature throughout the entire operation period. In other words, the extraction system maintains a constant pressure regardless of any fluctuations in the temperature of the fluid entering the system. The invariance in pressure displayed in the Figure 13 corroborates the model assumptions discussed in the Chapter X, where the pressure is assumed to be a control variable.

Figure 14 displays the sensitivity of the fluid enthalpy density to changes in the inlet temperature across the extraction bed over time. Given that the Dirichlet boundary conditions are applied to the system, any alteration in inlet temperature will have an immediate and localized effect on the enthalpy density at the entrance of the extraction column on the fluids enthalpy. This alteration results in a heat front propagation from the inlet to the outlet of the extractor as presented on the Figure 14. As time progresses, the impact of the inlet temperature on enthalpy diminish and the sensitivities converging towards zero. This convergence

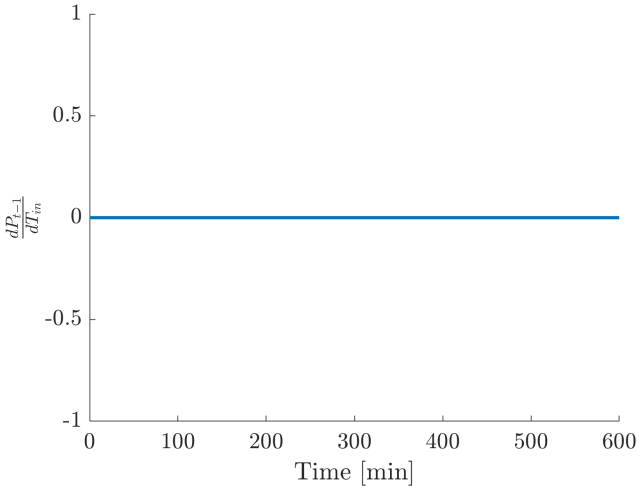

Figure 13: The effect of T_{in} change on P in the system

suggests that the system is reaching a new thermal equilibrium. The uniformity of the enthalpy at later times implies that the initial temperature perturbations have equilibrated throughout the bed, and the system has adapted to the new inlet temperature condition.

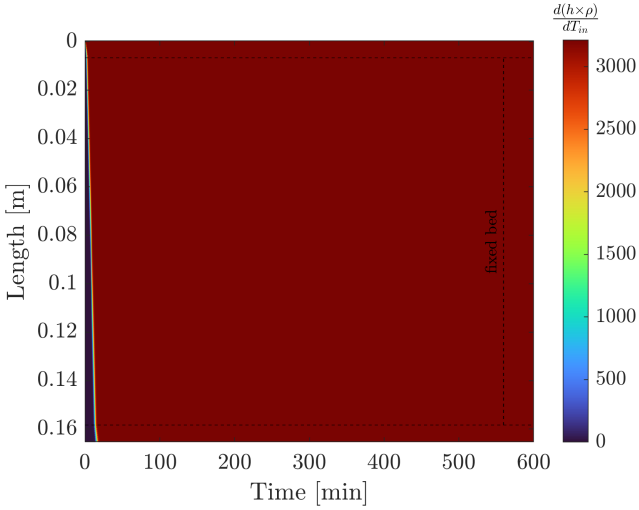

Figure 14: The effect of T_{in} change on $(h \times \rho)$ in the system

Figure 15 shows the temporal and spatial sensitivity of the solute concentration in the solid phase to changes in the inlet temperature during a supercritical fluid extraction process. The positive sensitivities observed suggest that the solute concentration in the solid phase increases with rising inlet temperature. This initial increase could be attributed to a reduction in solute solubility in the supercritical fluid at higher temperatures or a slowdown in mass transfer kinetics. As presented in article 1, a rise in temperature at constant pressure would increase solute diffusivity D_i^R in supercritical fluids; however, the increase in concentration in the solid phase indicates other dominating factors, such as changes in

solubility described by the solubility parameter (Υ), which might decrease, thereby reducing the extraction rate.

As the extraction progresses, the sensitivities flatten out and then decrease. Towards the end of the extraction period, the sensitivities approach a positive constant, implying that the effect of inlet temperature on the concentration of the solute in the solid phase becomes negligible. This behaviour can be explained if it assumed that the extraction kinetic slowed because at the high temperature, which leads to higher concentration gradient in the later part of the process. The reduced availability of extractable solute in the later part of the process corresponds to the diminishing of the sensitivity.

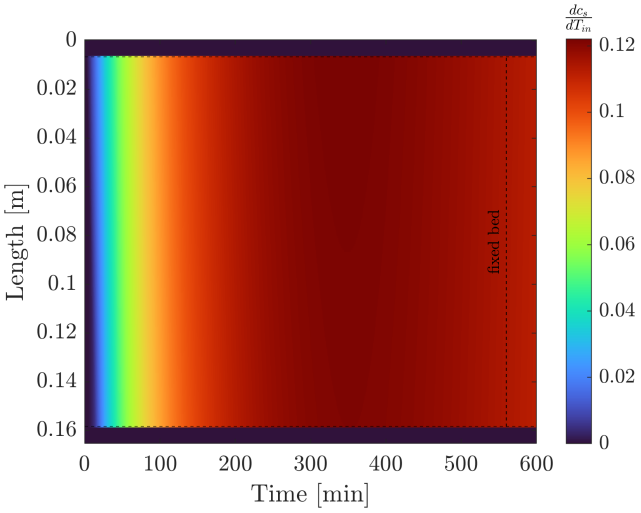

Figure 15: The effect of T_{in} change on C_s in the system

The Figure 16 represents the sensitivity of the concentration of solutes in the fluid phase over a period of 600 minutes as a result of changes in the inlet temperature. In the initial phase of the process, indicated by the area where sensitivities are at or near zero, there is a lack of response, likely reflecting an idle period or delay as the system adjusts to the new inlet temperature. This could represent the time needed for the thermal front to propagate through the system and influence the solubility and mass transfer rates of the solutes. As the warmer fluid begins to interact with the solid phase, the negative sensitivities are observed. These negative values imply a decrease in solute concentration within the fluid phase, which might be attributed to a reduced diffusion coefficient (D_i^R) due to increased fluid viscosity at higher temperatures, or possibly due to a change in the solubility (Υ) of the solute with temperature. If the solubility decreases with temperature for the given solute, an increase in temperature could indeed result in a lower solute concentration in the fluid phase. Later the sensitivities starts to increase due higher concentration gradient if compared to before the temperature change. Towards the end of the time period, the figure shows the sensitivities stabilizing at a constant value. Eventually, the system response stabilize around a constant value when the extraction kinetics become a limiting factor.

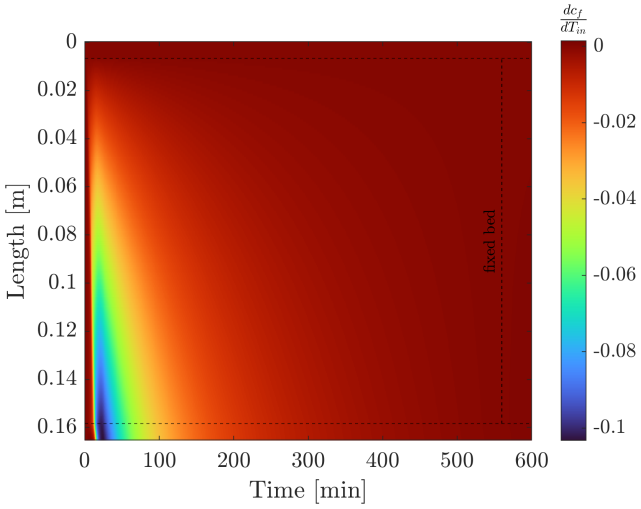

Figure 16: The effect of T_{in} change on C_f in the system

Figure 17 shows the time-dependent response of the extraction yield's sensitivity to changes in the inlet temperature. Initially, there is no change in yield as the heat front needs to propagate the along the system. That delayed response, cause the yield sensitivity to stay flat at the beginning of the extraction.

As the system starts responding, a small increase in sensitivity can be observed, which indicates a transient enhancement in yield. This is due to the velocity of the fluid, which is inversely proportional to density. The sensitivity peak comes from the fact that the fluid moves faster across the system, while the mass transfer kinetic is mainly driven by high concentration gradient.

Subsequently, the sensitivity curve descends into negative territory, suggesting that the increased inlet temperature eventually reduces the extraction efficiency. As explained above, due to complex relation between temperature and various mass transfer parameters, including the solubility of different compounds and the diffusivity within the supercritical fluid, the temperature increase might have a negatively affected on the extraction efficiency. The minimum point reached by the sensitivity curve implies a period where the yield is affected the most by the temperature increase.

Afterward, the curve's gradual ascent towards zero reflects a stabilizing effect. The curve eventually flattens out, maintaining a slightly negative sensitivity, suggesting that while the system has reached a new quasi-steady state. The overall yield remains slightly compromised compared to the baseline. At this point, the extraction process is limited by availability of the solute in the solid particles. This extended simulation offers a comprehensive view of how inlet temperature variations can impact the extraction yield over time.

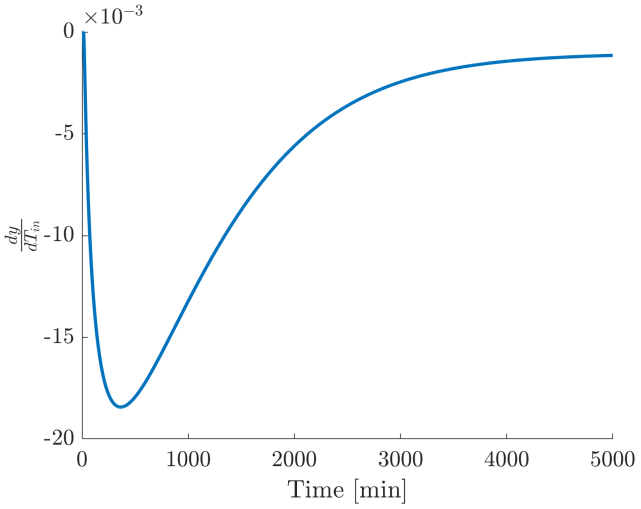

Figure 17: The effect of T_{in} change on $y(t)$ in the system

4. Conclusions

The sensitivity analysis is a tool to understand the parametric dependence in the dynamic behaviour of the analysed system. The presented formulation involves derivative-based local sensitivity analysis of the model solution with respect to selected parameters and controls. The sensitivity equations can be obtained in various ways, but the automatic differentiation technique was implemented to obtain the sensitivity equations in this work. By identifying which parameters are influential at each period of the simulation, local sensitivity analysis can yield valuable information for guiding the process modelling, the design of experiments or the model reduction. The local sensitivity analysis techniques consider the sensitivities at only a small region of parameter space, and the conclusions derived from such an analysis are limited to local conditions unless the discussed system is a linear model.

In this study, the local sensitivity analysis method was introduced to explore the dynamics of the supercritical extraction system, which consists of a set of partial differential equations. The sensitivity equations evaluate the influence of control variables such as flow rate, pressure, and inlet temperature on the state-space consisting of the concentration of the solute in solid and liquid phases, the fluid's enthalpy density, system pressure, and extraction yield. Every change in the control variables leads to a state-space change, eventually affecting the process performance.

Similarities between Figures 7, 12 and 17 can observed, although the sources of disturbances are different. All the plots stay initially plat, and this is because the extraction kinetic is mainly controlled by the concentration gradient. The largest sensitivity deviations are observed in the second extraction phase, which is mainly controlled by the internal mass transfer. These deviations are strongly related to the fluid velocity and the correlations used to connect the extraction kinetic parameters. As correlations used in this work are linear functions of the fluid density(article 1), Figures 12 and 17 are characterised by the opposite changes in the fluid density, which leads to the sensitivity plots with similar shape but opposite sign. In the third extraction phase, the concentration gradient and the internal diffusion coefficient decrease with the solute concentration in the solid phase(it is more difficult to extract the solute from the particle core than from the outer shell). It is important to note that the local-sensitivity methods obtain the discussed results, which can be obtained at different operating conditions.

This information can be utilized to identify which control variables influence the extraction yield the most. The controls with high sensitivities on the extraction can be used to investigate to find optimal operating conditions from an economic point of view.

References

[1] Ompal Singh, Zakia Khanam, Neelam Misra, and Manoj Kumar Srivastava. Chamomile (matricaria chamomilla l.): An overview. Pharmacognosy Reviews, 5(9):82, 2011. ISSN 0973-7847. doi: 10.4103/0973-7847.79103.

[2] Janmejai Srivastava. Extraction, characterization, stability and biological activity of flavonoids isolated from chamomile flowers. Molecular and Cellular Pharmacology, 1(3):138–147, August 2009. ISSN 1938-1247. doi: 10.4255/mcpharmacol.09.18.

[3] Anne Orav, Ain Raal, and Elmar Arak. Content and composition of the essential oil ofchamomilla recutita(l.) rauschert from some european countries. Natural Product Research, 24(1):48–55, January 2010. ISSN 1478-6427. doi: 10.1080/14786410802560690.

[4] Ernesto Reverchon, Giorgio Donsi, and Libero Sesti Osseo. Modeling of supercritical fluid extraction from herbaceous matrices. Industrial & Engineering Chemistry Research, 32(11):2721–2726, nov 1993. doi: 10.1021/ie00023a039.

[5] H. Sovova. Rate of the vegetable oil extraction with supercritical co2. modelling of extraction curves. Chemical Engineering Science, 49 (3):409–414, 1994. doi: 10.1016/0009-2509(94)87012-8.

[6] E. Reverchon. Mathematical modeling of supercritical extraction of sage oil. AIChE Journal, 42(6):1765–1771, June 1996. ISSN 1547-5905. doi: 10.1002/aic.690420627.

[7] L. Fiori, D. Calcagno, and P. Costa. Sensitivity analysis and operative conditions of a supercritical fluid extractor. The Journal of Supercritical Fluids, 41(1):31–42, may 2007. doi: 10.1016/j.supflu.2006.09.005.

[8] M.M. Santos, E.A. Boss, and R. Maciel Filho. Supercritical extraction of oleaginous: parametric sensitivity analysis. Brazilian Journal of Chemical Engineering, 17(4–7):713–720, December 2000. ISSN 0104-6632. doi: 10.1590/s0104-66322000000400035.

[9] Tahmasb Hatami and Ozan N. Ciftci. Techno-economic sensitivity assessment for supercritical co2 extraction of lycopene from tomato processing waste. The Journal of Supercritical Fluids, 204:106109, January 2024. ISSN 0896-8446. doi: 10.1016/j.supflu.2023.106109.

[10] Massimo Poletto and Ernesto Reverchon. Comparison of models for supercritical fluid extraction of seed and essential oils in relation to the mass-transfer rate. Industrial & Engineering Chemistry Research, 35(10):3680–3686, January 1996. ISSN 1520-5045. doi: 10.1021/ie9600093.

[11] John D. Anderson. Computational fluid dynamics the basic with applications. McGraw-Hill, 1995. ISBN 9780071132107.

[12] J. D. Jr Anderson. Fundamentals of Aerodynamics. McGraw-Hill Education, 2023. ISBN 9781264151929.

[13] N. R. Bulley, M. Fattori, A. Meisen, and L. Moyls. Supercritical fluid extraction of vegetable oil seeds. Journal of the American Oil Chemists' Society, 61(8):1362–1365, aug 1984. doi: 10.1007/bf02542243.

[14] M. Spiro and M. Kandiah. Extraction of ginger rhizome: partition constants and other equilibrium properties in organic solvents and in supercritical carbon dioxide. International Journal of Food Science & Technology, 25(5):566–575, jun 2007. doi: 10.1111/j.1365-2621.1990.tb01116.x.

[15] Helena Sovova. Broken-and-intact cell model for supercritical fluid extraction: Its origin and limits. The Journal of Supercritical Fluids, 129:3–8, nov 2017. doi: 10.1016/j.supflu.2017.02.014.

[16] Motonobu Goto, Bhupesh C. Roy, and Tsutomu Hirose. Shrinking-core leaching model for supercritical-fluid extraction. The Journal of Supercritical Fluids, 9(2):128–133, jun 1996. doi: 10.1016/s0896-8446(96)90009-1.

[17] A. Srinivasan and C. Depcik. One-dimensional pseudo-homogeneous packed-bed reactor modeling: I. chemical species equation and effective diffusivity. Chemical Engineering & Technology, 36(1):22–32, dec 2012. doi: 10.1002/ceat.201200458.

[18] J Elliott. Introductory chemical engineering thermodynamics. Prentice Hall, Upper Saddle River, NJ, 2011. ISBN 9780136068549.

[19] Jürgen Gmehling, Michael Kleiber, Bärbel Kolbe, and Jürgen Rarey. Chemical Thermodynamics for Process Simulation. Wiley, mar 2019. doi: 10.1002/9783527809479.

[20] H. Sovova, R. Komers, J. Kucuera, and J. Jezu. Supercritical carbon dioxide extraction of caraway essential oil. Chemical Engineering Science, 49(15):2499–2505, aug 1994. doi: 10.1016/0009-2509(94)e0058-x.

[21] Robert P. Dickinson and Robert J. Gelinas. Sensitivity analysis of ordinary differential equation systems—a direct method. Journal of Computational Physics, 21(2):123–143, jun 1976. doi: 10.1016/0021-9991(76)90007-3.

[22] Timothy Maly and Linda R. Petzold. Numerical methods and software for sensitivity analysis of differential-algebraic systems. Applied Numerical Mathematics, 20(1-2):57–79, feb 1996. doi: 10.1016/0168-9274(95)00117-4.

[23] Ding-Yu Peng and Donald B. Robinson. A new two-constant equation of state. Industrial & Engineering Chemistry Fundamentals, 15(1):59–64, feb 1976. doi: 10.1021/i160057a011.

EoS	u	w	a	b
van der Waals	0	0	$\frac{27}{64}\frac{R^2T_c^2}{P_c}$	$\frac{RT_c}{8P_c}$
Redlich and Kwong	1	0	$0.42748\frac{R^2T_c^{2.5}}{P_c}$	$\frac{0.08664RT_c}{P_c}$
Soave	1	0	$0.42748\frac{R^2T_c^2}{P_c}$	$\frac{0.08664RT_c}{P_c}$
Peng and Robinson [23]	2	-1	$0.45724\frac{R^2T_c^2}{P_c}$	$\frac{0.07780T_c}{P_c}$

Table 1
Parameters for Popular Cubic EoS

EoS	α	f(ω)
van der Waals	-	-
Redlich and Kwong	$\frac{1}{\sqrt{T_r}}$	-
Soave	$\left[1+f(\omega)\left(1-\sqrt{T_r}\right)\right]^2$	0.48+1.574ω-0.176ω^2
Peng and Robinson ([23])	$\left[1+f(\omega)\left(1-\sqrt{T_r}\right)\right]^2$	0.37464+1.54226ω-0.26992ω^2

Table 2
Parameters for Popular Cubic EoS

A. Appendix

A.1. Thermodynamic

A.1.1. Equation of state

A cubic equation of state (EoS) serves as a mathematical model to describe the behavior of real gases and liquids through a third-degree polynomial equation that correlates the pressure, volume, and temperature of a substance. These equations constitute tools for comprehending the phase behavior, properties, and thermodynamic processes of actual substances, across various engineering and scientific applications. The cubic equation of state take into account deviations from ideal gas behavior, which are particularly important at high pressures and low temperatures, where real gases do not follow assumption of ideal gas.

$$P = \frac{RT}{v_m - b} - \frac{\Phi}{v_m^2 - ubv_m + wb^2} \tag{31}$$

In this equation, P denotes the pressure of the substance, v_m represents the molar volume of the substance, T stands for the absolute temperature of the substance, u and w are integers that vary from one equation to another, R symbolizes the universal gas constant and ω denotes an acentric factor and $\Phi = a\alpha$.

The Van der Waals constants, constitute empirical values contingent upon the particular substance being modeled. These constants factor in molecular interactions (represented by 'a') and the finite size of gas molecules (indicated by 'b').

Several variations of the cubic equation of state exist, each with its own set of parameters and assumptions. Tables 1 and 2 show parameters for popular cubic EoS.

The general cubic equation of state can be represented as a polynomial, as indicated in Equation 32. In a one-phase region, the fluid is characterized by a single real root, corresponding to the gas, liquid, or supercritical phase. In the two-phase region, a gas-liquid mixture exists, and two roots are identified. The larger root corresponds to the gas phase, while the smaller root pertains to the liquid phase.

$$Z^3-(1+B-uB)Z^2+(A+wB^2-uB-uB^2)Z-AB-wB^2-wB^3 = 0 \tag{32}$$

where $A = \frac{\Phi P}{R^2T^2}$ and $B = \frac{bP}{RT}$.

If the Peng-Robinson equation of state (Peng and Robinson [23]) is used, the polynomial equation becomes

$$Z^3 - (1-B)Z^2 + (A - 2B - 3B^2)Z - (AB - B^2 - B^3) = 0 \tag{33}$$

For an ideal gas, the compressibility factor is defined as $Z = 1$, but the deviation of Z needs to be consider for real-life cases. The value of Z typically increases with pressure and decreases with temperature. At elevated pressures, molecules collide more frequently, allowing repulsive forces between molecules to influence the molar volume of the real gas (v_m) to surpass that of the corresponding ideal gas $\left(\left(v_m\right)_{ideal\ gas} = \frac{RT}{P}\right)$, resulting in Z exceeding one. At lower pressures, molecules move freely, with attractive forces predominating, leading to $Z < 1$.

Numerical methods such as Newton-Raphson can be used to solve the polynomial equation to obtain the compressibility $Z\left(T(t,z), P(t)\right)$ at given temperature and pressure. Alternatively, the closed form solution can by obtained by Cardano formula (Appendix A.2).

A.1.2. Density of the fluid phase

The density of the fluid can be calculated from the real gas equation $\rho = \frac{P}{RTZ}\frac{1}{m_{CO2}}$. The temperature can be obtain from the time evolution of governing equations, the pressure is consider to be constant along the system to be a know.

A.2. Cardano's Formula

Following the work of Gmehling et al. [19], a cubic equation of state can be written a following form

$$Z^3 + UZ^2 + SZ + T = 0 \tag{34}$$

with Z as the compressibility factor. Using Cardano's formula, this type of equation can be solved analytically.

$$P = \frac{3S - U^2}{3} \qquad Q = \frac{2U^3}{27} - \frac{US}{3} + T$$

the discriminant can be determined to be

$$D = \left(\frac{P}{3}\right)^3 + \left(\frac{Q}{2}\right)^2 \tag{35}$$

For $D > 0$, the equation of state has one real solution:

$$Z = \left[\sqrt{D} - \frac{Q}{2}\right]^{1/3} - \frac{P}{3\left[\sqrt{D} - \frac{Q}{2}\right]^{1/3}} - \frac{U}{3} \tag{36}$$

For $D < 0$, there are three real solutions:

$$\Theta = \sqrt{-\frac{P^3}{27}} \qquad \Phi = \arccos\left(\frac{-Q}{2\Theta}\right)$$

they can be written as

$$Z_1 = 2\Theta^(1/3)\cos\left(\frac{\Phi}{3}\right) - \frac{U}{3} \tag{37}$$

$$Z_2 = 2\Theta^(1/3)\cos\left(\frac{\Phi}{3} + \frac{2\pi}{3}\right) - \frac{U}{3} \tag{38}$$

$$Z_3 = 2\Theta^(1/3)\cos\left(\frac{\Phi}{3} + \frac{4\pi}{3}\right) - \frac{U}{3} \tag{39}$$

The largest and the smallest of the three values correspond to the vapor and to the liquid solutions, respectively. The middle one has no physical meaning.